中国激光

百瓦级中红外光纤随机激光放大

高旺城[1]，马瑞[1]，全欣[1]，陈宇[1]，范滇元[1]，刘军[1,2*]

[1]深圳大学微纳光电子学研究院二维材料光电科技国际合作联合实验室，广东 深圳 518060；

[2]中国科学院高功率激光物理重点实验室，上海 201800

摘要 中红外波段高功率激光光源在工业加工和生物医疗等领域中有着广泛的应用。报道了基于主振荡器功率放大器(MOPA)结构的百瓦级中红外连续波光纤随机激光器，获得了最高输出功率为100.40 W、斜率效率为47.8%、波长为1980 nm的连续波激光输出。得益于MOPA结构中光纤随机激光种子源在激光放大过程中的光谱带宽保持特性，100.40 W激光输出时的3 dB光谱带宽仅为~0.2 nm。激光器的短时时域强度波动和长时功率波动均表现出优良的稳定性。所提实验技术方案和实验结果有望进一步拓宽中红外高功率光纤随机激光器的应用范围。

关键词 激光器；光纤随机激光器；高功率激光器；瑞利散射；中红外激光器；高稳定性

中图分类号 O436 **文献标志码** A **DOI**：10.3788/CJL230874

1 引 言

近年来，光纤随机激光器(RFL)发展迅速[1-3]。区别于传统谐振腔型的光纤激光器，RFL中的开放腔结构和非相干反馈使得输出激光的时域动态无谐振纵模且强烈受抑制。目前，RFL的相关研究主要聚焦在高功率/高效率产生[4-7]、超宽带多波长激射[8-9]、窄线宽输出[10-11]、超连续谱产生[12-14]、分布式光放大[15]以及成像光源[16-17]等功能实现方面，已取得了一系列成果。值得注意的是，受限于中红外波段激光在石英光纤中的较大传输损耗和较弱的瑞利散射效应，RFL的工作波长仍主要集中在近红外波段(1.1~1.7 μm)[18-20]。因此，进一步拓宽光纤随机激光器的工作波长范围并提升其输出性能具有重要的科学意义和应用价值。

2 μm波段激光处于水分子吸收峰处，包含许多重要分子的特征谱线，在精密加工、环境检测、生物医疗等方面有着重要应用[21-24]。近年来，基于传统有源谐振腔的2 μm光纤激光器在高功率激光输出[25-26]、波长可调谐输出[27-28]、单频激光输出[29-30]等方面都取得了极大进展。但是，该腔型光纤激光器在结构紧凑性和输出激光时域稳定性等方面仍需进一步优化提升。近年来，深圳大学的Ma等[31]开展了基于无源反馈结构的中红外波段光纤随机激光器研究，对比了三种不同腔型结构下的2 μm光纤激光器，包括无源反馈半开放腔结构、单通放大结构和常规谐振腔结构，获得了时域动态极其稳定的随机激光输出。此外，中红外光纤随机激光器的相关研究还包括脉冲泵浦产生2.1 μm激光[32]、基于非线性频率转换产生中红外激光[9,33-34]、基于氟化物光纤的中红外随机激光的理论仿真和优化设计[35]以及基于光纤随机光栅产生中红外激光[36-37]等。已报道的相关研究工作所涉及的中红外光纤随机激光器的输出激光较弱。因此，须进一步提升中红外光纤随机激光器的输出功率以满足相关应用要求。本文提出了一种基于主振荡器功率放大器(MOPA)结构的2 μm高功率光纤随机激光器。激光器的最高输出功率为100.40 W，斜率效率为47.8%。同时，输出激光的短时时域和长时功率波动均表现出优良的稳定性。受益于MOPA结构中光纤随机激光种子源在激光放大过程中的光谱带宽保持特性，激光器在高功率运转时仍保持窄线宽输出特性。研究结果为2 μm高功率光纤随机激光器的优化设计提供了思路，并有望进一步拓展其应用范围。

2 实验结构

基于MOPA结构的1980 nm光纤随机激光器的实验装置如图1所示。该装置种子源是基于前向泵浦的半开放腔结构，其增益由有源掺铥光纤提供，激光腔反馈由普通单模光纤(SMF)中的随机分布瑞利散射和光纤布拉格光栅(FBG)中的点反射共同提供。种子源中793 nm半导体激光(LD)经由(2+1)×1合束

收稿日期：2023-05-31；**修回日期**：2023-07-09；**录用日期**：2023-08-14；**网络首发日期**：2023-09-15

基金项目：中国科学院高功率激光物理重点实验室开放基金(SGKF202107)、广东省基础与应用基础研究基金(2022A1515010326，2021A1515011532，2020A1515110471，2020A1515111143)、深圳市科技创新委员会优青项目(RCYX20210609103157071)、深圳市科技创新委员会重点项目(JCYJ20220818100019040)

通信作者：*liu-jun-1987@live.cn

器的泵浦端进入至2.4 m长的掺铥光纤(TDF)中并对其进行泵浦。该LD的最大输出功率为30 W,输出尾纤的纤芯/包层直径分别为105 μm/125 μm,数值孔径(NA)为0.22。TDF在793 nm处的包层泵浦吸收为9.00 dB/m,纤芯直径和NA分别为10 μm和0.150,内包层直径和NA分别为130 μm和0.46。在合束器的信号端口熔接1980 nm高反射率(HR)的FBG(反射率大于99%,3 dB带宽为0.2 nm)作为点式反射器及波长选择器。TDF远端则熔接一段200 m长的SMF以提供非相干光反馈。值得注意的是,与近红外波段激光相比,中红外激光在SMF中传输时具有更高的传输损耗和更低的瑞利散射系数。SMF长度(200 m)的选择须兼顾SMF中传输损耗和瑞利散射强度的平衡。SMF远端连接一个光纤隔离器(ISO)以防止逆向光回返损伤器件及影响种子源稳定性。种子源输出信号光经另一个(2+1)×1合束器进入前置放大级,前置放大级增益光纤为一段2.4 m长的与种子源中的增益光纤同类型的TDF,前置放大级泵浦源为793 nm LD,其最大输出功率为50 W,输出尾纤纤芯/包层直径分为105 μm/125 μm,纤芯NA为0.22。前置放大级中的TDF末端同样连接一个ISO以隔离反射光。由于种子源输出功率较小,前置放大级的作用是进一步提高信号光功率,满足主放大级中高效增益提取和功率放大的要求。前置放大级和主放大级之间插入一个模场适配器(MFA)以降低不同类型光纤间的模式不匹配所引入的插入损耗。前置放大级输出信号光经(6+1)×1合束器进入4.7 m长的大模场掺铥光纤(LMA-TDF)以实现百瓦级功率输出。(6+1)×1合束器的泵浦端光纤为多模光纤,其信号端和输出端光纤均为双包层光纤。LMA-TDF在793 nm处的包层泵浦吸收为2.00 dB/m,纤芯直径和NA分别为25 μm和0.09,内包层直径和NA分别为400 μm和0.46。主放大级中的泵浦源由两个高功率793 nm LD提供,单个LD最大输出功率为140 W,纤芯/包层直径分为200 μm/220 μm,纤芯NA为0.22。LMA-TDF的尾端连接泵浦光剥离器(CPS)。为减少量子亏损导致的热负荷的影响,所有增益光纤均置于水冷板上,其中种子源与前置放大级中的增益光纤所在的水冷板温度设定为20 ℃,主放大级中增益光纤所在的水冷板的温度设定为10 ℃。主放大级中增益光纤的盘绕直径为~10 cm,以此抑制高阶模的产生。实验中TDF增益光纤长度(2.4 m)和LMA-TDF增益光纤长度(4.7 m)主要由其对应泵浦吸收系数及实验室库存光纤长度综合决定,以便获得高的光光转换效率和输出功率。激光输出性能参数分别由光谱分析仪、功率计、光电探测器、示波器和射频(RF)频谱分析仪监测。

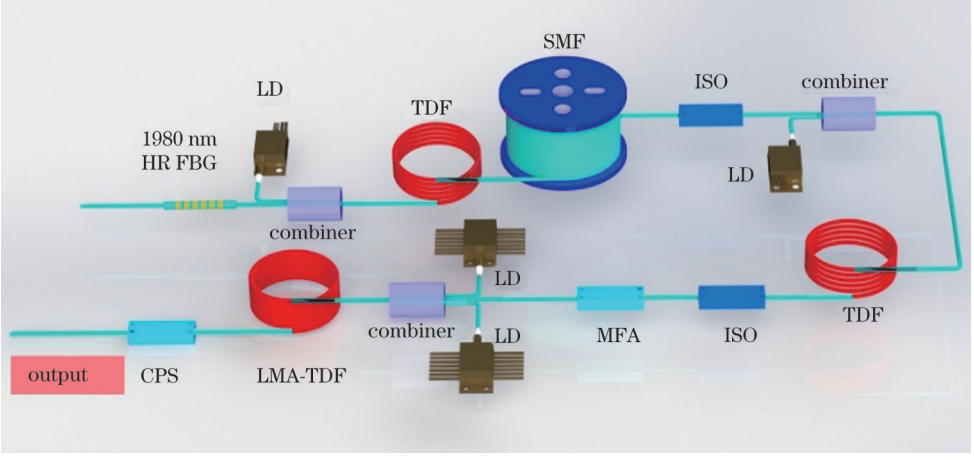

图1 1980 nm光纤随机激光器实验装置图

Fig. 1 Experimental setup of 1980 nm random fiber laser

3 实验结果与讨论

首先,开展了光纤随机激光器种子源特性研究。图2(a)给出了种子源输出功率与泵浦功率的关系曲线图。可以看出:激光阈值约为3.57 W,斜率效率约为13.6%;泵浦功率为7.40 W时的最大输出功率为0.524 W。输出功率的进一步提升受时域不稳定寄生激光产生的限制[31]。图2(b)给出了不同泵浦功率下的输出激光光谱图。可以看出:不同泵浦功率下的光谱稳定光滑,无显著的光谱展宽,这与基于纯拉曼增益机制的传统RFL有所不同[19]。主要归因于两方面:其一,种子源输出功率很低,非线性效应不明显;其二,2 μm波段激光远离SMF的零色散波长(ZDW,~1.3 μm),该波段激光在SMF中无显著的非线性光谱展宽效应。与传统谐振腔型激光器相比,基于非相干反馈的RFL表现出强烈的短时时域动态抑制特性。时域特性如图2(c)所示,采用标准差除以平均值(A)来表征输出激光的时域动态特性。结果表明,种子源时域波动表现出高度稳定性,当最大泵浦功率为7.40 W时,A值为0.0256,这主要归因于种子源的半开腔非谐振结构[31]。图2(d)给出了种子源在7.40 W泵浦功率下的射频频谱(视频带宽为300 Hz),与光电探测器

(PD)的固有噪声基底相比，只有较低的频率分量略有增加，在整个频率带宽内未观察到共振频率。结果表明，1980 nm 光纤随机激光器种子源具有优异的激光性能，在 MOPA 结构中满足实现高功率 RFL 的要求。

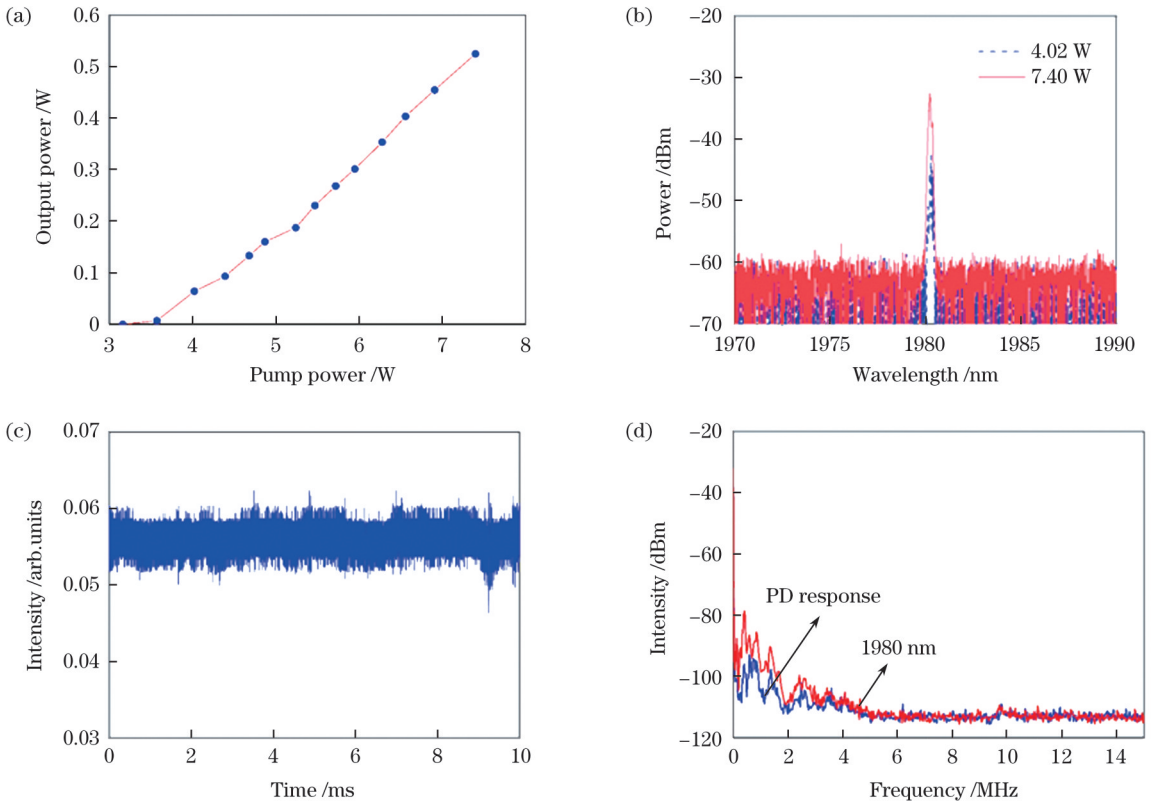

图 2　光纤随机激光器种子源特性。(a)输出功率与泵浦功率的关系曲线；(b)不同泵浦功率下的光谱；(c) 7.40 W 泵浦功率下的短时时域轨迹；(d) 7.40 W 泵浦功率下的射频谱

Fig. 2　Characteristics of seed source of RFL. (a) Output power versus pump power; (b) spectra at different pump powers; (c) short-time temporal trace at pump power of 7.40 W; (d) radio frequency spectrum at pump power of 7.40 W

种子源激光输出功率设为 0.286 W，然后将其注入至前置放大级中进行放大。前置放大级输出特性如图 3 所示。图 3(a)表示前置放大级中输出功率和泵浦功率的关系曲线：当泵浦功率为 8.96 W 时，前置放大级的最大输出功率为 3.09 W，斜率效率为 35.6 %。图 3(b)表示前置放大级的输出激光在不同泵浦功率下的输出光谱图。可以看出：与种子源输出光谱类似，光谱分布保持稳定光滑，无明显展宽现象，这主要受益于 MOPA 结构中光纤随机激光种子源在激光放大过程中的光谱带宽保持特性[18]。

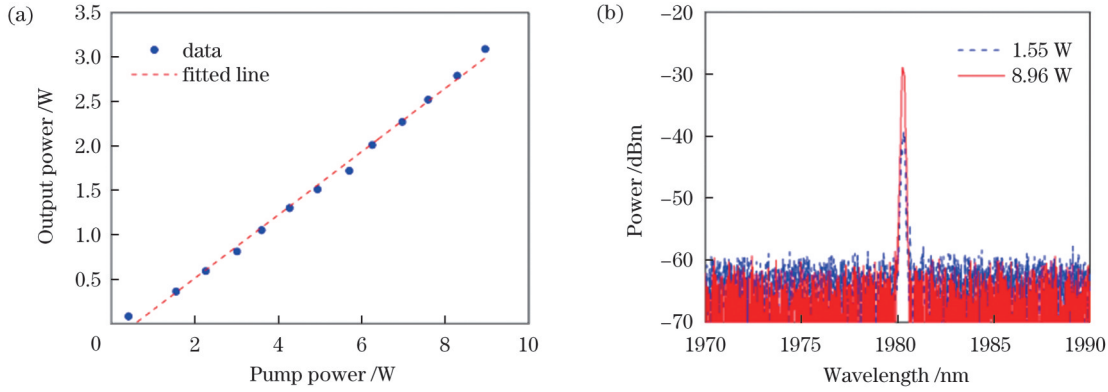

图 3　光纤随机激光器中前置放大器的输出特性。(a)输出功率与泵浦功率的关系曲线；(b)不同泵浦功率下的输出光谱图

Fig. 3　Output characteristics of preamplifier in RFL. (a) Output power versus pump power; (b) spectra at different pump powers

前置放大级输出的～3.09 W 信号光通过 MFA 注入到主放大级中。主放大级泵浦源为两个高功率的 793 nm LD，增益光纤为 4.7 m 长的 LMA-TDF，最终输出百瓦级 1980 nm 随机激光。主放大级输出功率与注入的泵浦功率的关系曲线如图 4 所示。泵浦功率为 215.7 W 时的最大输出功率为 100.40 W，斜率效率为

47.8%，输出功率曲线无明显饱和趋势，输出功率的进一步提升主要受限于泵浦光源和实验室水冷系统。

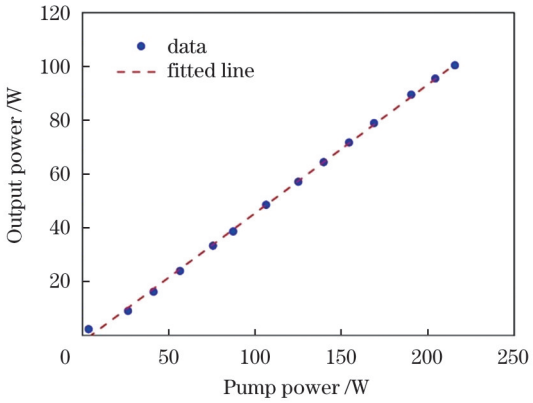

图 4 光纤随机激光器主放大器中输出功率与泵浦功率的关系

Fig. 4 Output power versus pump power in main amplifier of RFL

光纤随机激光器主放大级的输出光谱特性如图 5 所示。图 5(a)给出了不同泵浦功率下的输出光谱。当输出功率从 40.00 W 增加到 100.40 W 时，输出光谱仍保持窄线宽特征。这主要得益于以光纤随机激光器作为种子源的 MOPA 结构的光谱带宽保持特性[18, 38-39]：基于半开放腔结构的光纤随机激光种子源的相对强度波动较小，从而抑制了激光放大过程中高峰值功率脉冲相关联的非线性效应；此外，主放大级中大模场增益光纤的使用也大大削弱了放大过程中的非线性效应，从而使得输出激光光谱带宽基本保持不变。图 5(b)给出了不同泵浦功率下 3 dB、10 dB 输出光谱带宽的变化。当输出功率从 10.33 W 增加到 100.40 W 时，3 dB 带宽仅从～0.13 nm 略微展宽到～0.20 nm，而 10 dB 带宽从～0.29 nm 展宽到～0.32 nm，证明可利用基于窄线宽 RFL 种子源的 MOPA 结构来实现高功率、窄线宽的中红外随机激光输出。

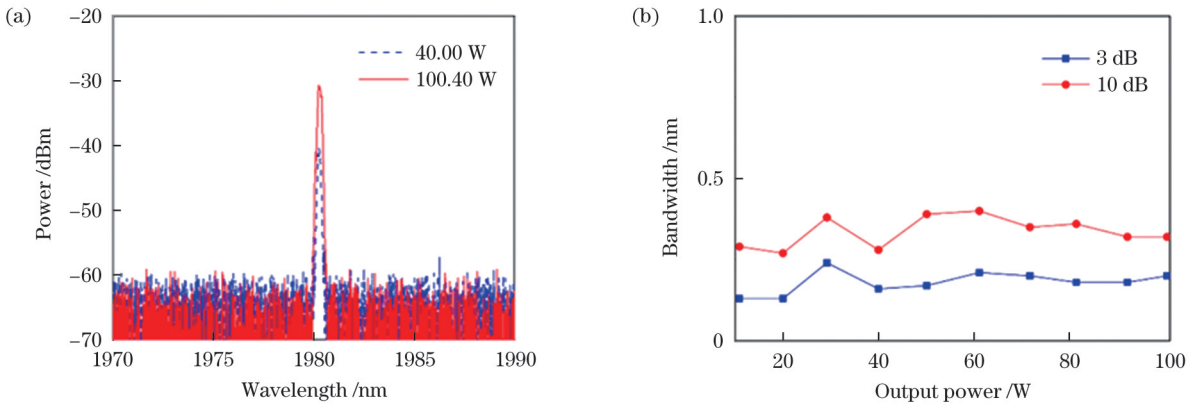

图 5 光纤随机激光器主放大器的光谱特性。(a)不同输出功率下的光谱；(b)不同输出功率下的 3 dB、10 dB 带宽

Fig. 5 Spectrum characteristics of main amplifier of RFL. (a) Spectra at different output powers; (b) 3 dB and 10 dB bandwidths at different output powers

图 6 进一步从时域和频域的角度分析了主放大级中光纤随机激光器的稳定性。受益于半开放腔非谐振结构，时域波动受到强烈抑制，如图 6(a)所示，随着输出功率从 20.00 W 增加到 100.40 W，由分布式随机瑞利散射引入的非相干反馈过程会进一步抑制时域动态过程，A 值从 0.1419 降低到 0.0319，时域波动较小。主放大级中 1980 nm RFL 的射频谱(视频带宽为 300 Hz)如图 6(b)所示，与 1980 nm 光纤随机激光器种子源特

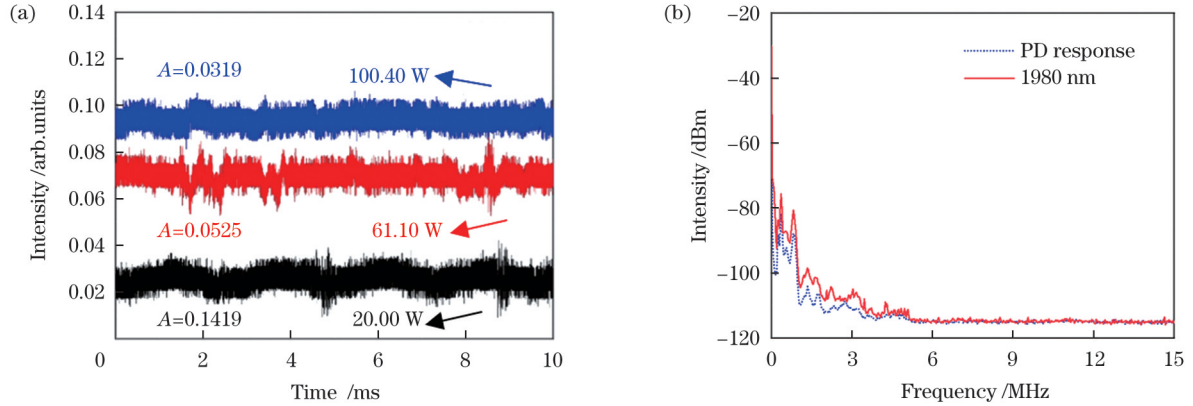

图 6 光纤随机激光器主放大器的输出特性。(a)不同输出功率下的短时时域强度分布；(b)最大泵浦功率下的射频谱

Fig. 6 Output characteristics of main amplifier of RFL. (a) Short-time temporal intensity distributions at different output powers; (b) radio frequency spectrum at maximum pump power

征类似，在整个频谱范围内未观察到共振频率，这表明该激光腔结构仍能保持典型的随机激光输出。最后测试了当输出功率约为 72 W 时，30 min 内 1980 nm 随机激光输出功率的长时间波动情况，如图 7 所示。得到的 A 值为 0.0048，表明基于 MOPA 结构的光纤随机激光器具有优良的长时功率稳定性。因此，在测量单点泵浦功率对应的输出功率时，我们只记录了均值。上述结果表明，所获得的高功率 1980 nm 光纤随机激光器具有典型的随机结构特性和较好的时间稳定性，有利于拓展中红外波段高功率随机激光的应用范围。

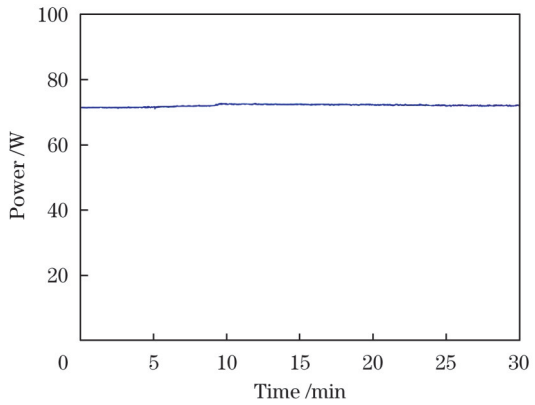

图 7 光纤随机激光器的长时间输出功率稳定性

Fig. 7 Stability of long time output power of RFL

4 结 论

基于 MOPA 结构的 RFL 实现了最高输出功率为 100.40 W 的 2 μm 光纤随机激光输出。得益于随机激光的独特优势，输出的高功率随机激光具有较窄的线宽：输出功率为 100.40 W 时 3 dB 带宽仅为～0.2 nm，输出激光的短时时域强度波动和长时功率波动均较小，装置具有较高的稳定性。总之，建立的基于 MOPA 结构的中红外光纤随机激光器实现了高功率窄线宽随机激光输出，为实现 2 μm 波段高性能激光光源提供了一种解决方案。

参 考 文 献

[1] Turitsyn S K, Babin S A, El-Taher A E, et al. Random distributed feedback fibre laser[J]. Nature Photonics, 2010, 4(4): 231-235.

[2] Churkin D V, Sugavanam S, Vatnik I D, et al. Recent advances in fundamentals and applications of random fiber lasers[J]. Advances in Optics and Photonics, 2015, 7(3): 516-569.

[3] Gomes A S L, Moura A L, de Araújo C B, et al. Recent advances and applications of random lasers and random fiber lasers[J]. Progress in Quantum Electronics, 2021, 78: 100343.

[4] Wang Z H, Yan P, Huang Y S, et al. An efficient 4-kW level random fiber laser based on a tandem-pumping scheme[J]. IEEE Photonics Technology Letters, 2019, 31(11): 817-820.

[5] Zhang H W, Huang L, Song J X, et al. Quasi-kilowatt random fiber laser[J]. Optics Letters, 2019, 44(11): 2613-2616.

[6] Wang Z N, Wu H, Fan M Q, et al. High power random fiber laser with short cavity length: theoretical and experimental investigations [J]. IEEE Journal of Selected Topics in Quantum Electronics, 2015, 21(1): 10-15.

[7] Vatnik I D, Churkin D V, Podivilov E V, et al. High-efficiency generation in a short random fiber laser[J]. Laser Physics Letters, 2014, 11(7): 075101.

[8] Zhang L, Jiang H W, Yang X Z, et al. Nearly-octave wavelength tuning of a continuous wave fiber laser[J]. Scientific Reports, 2017, 7: 42611.

[9] Wu H, Wang W Z, Li Y, et al. Difference-frequency generation of random fiber lasers for broadly tunable mid-infrared continuous-wave random lasing generation[J]. Journal of Lightwave Technology, 2022, 40(9): 2965-2970.

[10] Leandro D, Rota-Rodrigo S, Ardanaz D, et al. Narrow-linewidth multi-wavelength random distributed feedback laser[J]. Journal of Lightwave Technology, 2015, 33(17): 3591-3596.

[11] Zhang L, Wang C, Li Z Y, et al. High-efficiency Brillouin random fiber laser using all-polarization maintaining ring cavity[J]. Optics Express, 2017, 25(10): 11306-11314.

[12] He J R, Song R, Tao Y, et al. Supercontinuum generation directly from a random fiber laser based on photonic crystal fiber[J]. Optics Express, 2020, 28(19): 27308-27315.

[13] Ma R, Zhang W L, Wang S S, et al. Simultaneous generation of random lasing and supercontinuum in a completely-opened fiber structure[J]. Laser Physics Letters, 2018, 15(8): 085111.

[14] Ma R, Rao Y J, Zhang W L, et al. Backward supercontinuum generation excited by random lasing[J]. IEEE Journal of Selected Topics in Quantum Electronics, 2018, 24(3): 0901105.

[15] Fu Y, Zhu R C, Han B, et al. 175-km repeaterless BOTDA with hybrid high-order random fiber laser amplification[J]. Journal of Lightwave Technology, 2019, 37(18): 4680-4686.

[16] Wu H, Han B, Wang Z N, et al. Temporal ghost imaging with random fiber lasers[J]. Optics Express, 2020, 28(7): 9957-9964.

[17] Ma R, Rao Y J, Zhang W L, et al. Multimode random fiber laser for speckle-free imaging[J]. IEEE Journal of Selected Topics in Quantum Electronics, 2019, 25(1): 0900106.

[18] Wu H, Wang Z N, He Q H, et al. Common-cavity ytterbium/Raman random distributed feedback fiber laser[J]. Laser Physics Letters, 2017, 14(6): 065101.

[19] Ma R, Quan X, Wu H, et al. 20 watt-level single transverse mode narrow linewidth and tunable random fiber laser at 1.5 μm band[J]. Optics Express, 2022, 30(16): 28795-28804.

[20] Quan X, Ma R, Wu H, et al. Low threshold and high spectral purity 1.7 μm random fiber laser based on hybrid gain[J]. Optics & Laser Technology, 2022, 155: 108410.

[21] Mingareev I, Weirauch F, Olowinsky A, et al. Welding of polymers using a 2 μm thulium fiber laser[J]. Optics & Laser Technology, 2012, 44(7): 2095-2099.

[22] Ren X Y, Dai H, Li D T, et al. Mid-infrared electro-optic dual-comb spectroscopy with feedforward frequency stepping[J]. Optics Letters, 2020, 45(3): 776-779.

[23] Hardy L A, Wilson C R, Irby P B, et al. Rapid thulium fiber laser lithotripsy at pulse rates up to 500 Hz using a stone basket[J]. IEEE Journal of Selected Topics in Quantum Electronics, 2014, 20(5): 138-141.

[24] Hao Q, Zhu G S, Yang S, et al. Mid-infrared transmitter and receiver modules for free-space optical communication[J]. Applied Optics, 2017, 56(8): 2260-2264.

[25] Zhang Z, Shen D Y, Boyland A J, et al. High-power Tm-doped fiber distributed-feedback laser at 1943 nm[J]. Optics Letters, 2008, 33(18): 2059-2261.

[26] Yin K, Zhang B, Xue G H, et al. High-power all-fiber wavelength-tunable thulium doped fiber laser at 2 μm[J]. Optics Express, 2014, 22(17): 19947-19952.

[27] Li J F, Sun Z Y, Luo H Y, et al. Wide wavelength selectable all-fiber thulium doped fiber laser between 1925 nm and 2200 nm[J]. Optics Express, 2014, 22(5): 5387-5399.

[28] Yin K, Zhu R Z, Zhang B, et al. 300 W-level, wavelength-widely-tunable, all-fiber integrated thulium-doped fiber laser[J]. Optics

Express, 2016, 24(10): 11085-11090.
[29] Zhang Q, Hou Y B, Wang X, et al. 5 W ultra-low-noise 2 μm single-frequency fiber laser for next-generation gravitational wave detectors[J]. Optics Letters, 2020, 45(17): 4911-4914.
[30] Liu Y Z, Cao C, Xing Y B, et al. 406 W narrow-linewidth all-fiber amplifier with Tm-doped fiber fabricated by MCVD[J]. IEEE Photonics Technology Letters, 2019, 31(22): 1779-1782.
[31] Ma R, Liu J, Fang Z Q, et al. Mid-infrared random fiber laser assisted by the passive feedback[J]. Journal of Lightwave Technology, 2021, 39(15): 5089-5095.
[32] Jin X X, Lou Z K, Zhang H W, et al. Random distributed feedback fiber laser at 2.1 μm[J]. Optics Letters, 2016, 41(21): 4923-4926.
[33] Wu H S, Wang P, Song J X, et al. High power tunable mid-infrared optical parametric oscillator enabled by random fiber laser [J]. Optics Express, 2018, 26(5): 6446-6455.
[34] Wu H, Wang W Z, Hu B, et al. Widely tunable continuous-wave visible and mid-infrared light generation based on a dual-wavelength switchable and tunable random Raman fiber laser[J]. Photonics Research, 2023, 11(5): 808-816.
[35] Tian Y, Yao T F, Zhou P, et al. Numerical modeling and optimization of mid-infrared random distributed feedback fiber lasers[J]. Laser Physics, 2018, 28(7): 075104.
[36] Zhou L W, Hu Y Z, Zheng W L, et al. Triple-wavelength thulium-doped fiber random laser based on random fiber grating[J]. Photonics, 2023, 10(4): 355.
[37] 胡耀宗, 朱德才, 黄昌清, 等. 基于随机光栅的掺铥光纤随机激光器研究[J]. 中国激光, 2023, 50(2): 0201002.
Hu Y Z, Zhu D C, Huang C Q, et al. Study on thulium-doped fiber random laser based on random grating[J]. Chinese Journal of Lasers, 2023, 50(2): 0201002.
[38] Du X Y, Zhang H W, Ma P F, et al. Kilowatt-level fiber amplifier with spectral-broadening-free property, seeded by a random fiber laser[J]. Optics Letters, 2015, 40(22): 5311-5314.
[39] Wang Z H, Yu W L, Tian J D, et al. 5.1 kW tandem-pumped fiber amplifier seeded by random fiber laser with high suppression of stimulated Raman scattering[J]. IEEE Journal of Quantum Electronics, 2021, 57(2): 6800109.

Hundred-Watt-Level Mid-Infrared Random Fiber Laser Amplifier

Gao Wangcheng[1], Ma Rui[1], Quan Xin[1], Chen Yu[1], Fan Dianyuan[1], Liu Jun[1,2*]

[1]*International Collaborative Laboratory of 2D Materials for Optoelectronics Science and Technology, Institute of Microscale Optoelectronics, Shenzhen University, Shenzhen* 518060, *Guangdong, China*;

[2]*Key Laboratory of High Power Laser and Physics, Chinese Academy of Sciences, Shanghai* 201800, *China*

Abstract

Objective High-power laser sources operating in 2-μm band are gaining traction due to their diverse applications, including laser scalpels, plastic welding, and free-space laser communication. Over the past decade, random fiber lasers (RFLs) have emerged as a focal point of interest. These lasers utilize randomly distributed Rayleigh scattering and nonlinear amplification, distinguishing them from traditional resonant cavity lasers. The defining features of RFLs are their open cavity structure and incoherent feedback, which result in modeless lasing and significant suppression of temporal dynamics. However, research on RFLs has primarily concentrated on the near-infrared band, specifically around 1.1 μm and 1.5 μm, due to challenges such as significant transmission loss and weaker Rayleigh scattering in mid-infrared silica-based optical fibers. Historically, RFLs in the mid-infrared band have only realized low power outputs. In this study, we introduce a high-power RFL operating at 2 μm, utilizing the master oscillator power amplifier (MOPA) approach. Impressively, we realize a peak power of 100.40 W with an efficiency slope of 47.8% and a narrow 3 dB spectral width of approximately 0.2 nm.

Methods Figure 1 depicts the experimental arrangement for a high-powered RFL using the MOPA design. The seed consists of a 793-nm laser diode (LD), a (2+1)×1 pump combiner, a 2.4-m long thulium-doped fiber, a 1980-nm FBG, a 200-m single-mode fiber (SMF), and an isolator (ISO). The 1980-nm FBG serves as a point reflector, selecting the wavelength and providing optical feedback, in tandem with the Rayleigh scattering in the extended SMF. An isolator at the SMF end prevents unwanted light reflection. The preamplifier stage consists of a 793-nm LD, (2+1)×1 pump combiner, a 2.4-m thulium-doped fiber, and an isolator. Its role is to enhance the seed laser output power to a specified threshold. Inserting a mode-field adaptor (MFA) between the preamplifier and main amplifier minimizes insertion loss due to mode mismatch among different fibers. The main amplifier takes the laser signal from the MFA and amplifies it using a (6+1)×1 combiner and 4.7-m long large-mode-area thulium-doped fiber (LMA-TDF). This configuration facilitates a lasing output in the 100-W range, powered by two 793-nm high-intensity LDs. To remove residual pump light, a cladding power stripper (CPS) is integrated at the LMA-TDF terminal. Its endpoint is oriented to counter unintended feedback from the Fresnel reflection. Lastly, all gain fibers are positioned on a water-cooled plate for thermal efficiency. In the main amplifier stage, these fibers are coiled to approximately 10 cm in diameter, mitigating high-order transverse modes.

Results and Discussions The RFL seeds exhibit superior lasing characteristics, which encompass a narrow spectral linewidth and exceptional temporal stability. The threshold pump power for the seed source is determined as approximately 3.57 W, with a slope efficiency of 13.6%. The standard deviation divided by the mean value (A) stands at 0.0265 with a maximum pump power of 7.40 W. This is primarily attributed to the half-opened, non-resonant structure of the seed, in contrast to a resonant cavity (Fig. 2). The preamplifier stage further boosts the output power. At a pump power of 8.96 W, the maximum output power from the preamplifier stage is 3.09 W, having a slope efficiency of 35.6%. Importantly, the output spectrum of the preamplifier stage retains its narrow

linewidth feature. This is a benefit of the spectral-broading-free characteristic when the random fiber laser serves as the seed in the MOPA configuration (Fig. 3). In the main amplification stage, a hundred-watt-level mid-infrared lasing output materializes. With a pump power of 215.7 W, the maximum output power corresponds to 100.40 W and demonstrates a slope efficiency of 47.8%. No decline in the output power is evident, and potential for further power enhancement is predominantly constrained by laboratory cooling conditions and available pump sources (Fig. 4). Notably, the output spectrum of the main amplification stage also upholds a narrow linewidth, which benefits from the unique spectral broadening-free attribute of the power amplification process founded on a half-open-cavity seed. The RFL seed output power showcases extremely minimal power fluctuations, leading to suppressed nonlinear effects. Moreover, the inclusion of a large-mode-field gain fiber in the main amplification stage aids in curtailing nonlinear effects. There is no evident spectral broadening as the output power increases from 10.33 W to 100.40 W in terms of 3 dB and 10 dB bandwidths. The 3 dB spectral bandwidth at an output power of 100.40 W is approximately 0.2 nm (Fig. 5). The final laser output also demonstrates remarkable stability in short and long durations. This stability arises from the suppressed temporal dynamics induced by the incoherent feedback process via randomly distributed Rayleigh scattering. The A value decreases from 0.1419 to 0.0319 as the output power increases from 20.00 W to 100.40 W (Fig. 6). Furthermore, the output power fluctuation at approximately 72 W, in terms of the A value over a 30-min interval, is only 0.0048 (Fig. 7).

Conclusions In this study, a high-power RFL in 2-μm band is realized using the MOPA configuration. Due to the distinctive properties of the random laser, a lasing output with a remarkably narrow linewidth (approximately 0.2 nm) is obtained. The short-term domain dynamics and long-term power fluctuations of the lasing display excellent stability. This study offers a compelling alternative for crafting a high-performance random laser source in 2-μm band.

Key words lasers; random fiber lasers; high power lasers; Rayleigh scattering; mid-infrared lasers; high stability